

Supporting Information

Metal organic framework derived low-crystallized cobalt-nitrogen-carbon electrocatalysts for nitrate reduction to ammonia

Yue Cao, Shengbo Yuan, Wenbo Zhou, Yan Hai, Xiaoman Li, * and Min Luo*

State Key Laboratory of High-efficiency Utilization of Coal and Green Chemical Engineering, School of Chemistry and Chemical Engineering, Ningxia University, Yinchuan, Ningxia 750021, P. R. China

E-mail: luominjy@nxu.edu.cn, lixm2017@nxu.edu.cn

Contents

1. Figure S 1. (a) UV-Vis absorption curves of NO_3^- -N. (b) Calibration curve used to estimate the concentrations of NO_3^- -N.	3
2. Figure S 2. (a) UV-Vis absorption curves of NO_2^- -N. (b) Calibration curve used to estimate the concentrations of NO_2^- -N.	4
3. Figure S 3. (a) UV-Vis curves of various concentrations of N_2H_4 stained with $\text{C}_9\text{H}_{11}\text{NO}$ indicator. (b) A calibration curve used to estimate the concentrations of N_2H_4	5
4. Figure S 4. (a) UV-Vis absorption curves of Nessler's reagent assays kept with different concentrations of NH_4^+ -N. (b) Calibration curve used to estimate the concentrations of NH_4^+ -N.	6
5. Figure S 5. The NH_4^+ detection of (a) standard spectra and (b) fitting curve by ion chromatography.....	7
6. Figure S 6. The XRD patterns of the Co-MOF precursor.....	9
7. Figure S 7. The XRD patterns of the Co-N-C-500, Co-N-C-600, Co-N-C-700, and Z-Co-N-C-900.....	9
8. Figure S 8. The XRD patterns of the Co-N-C-400, Co-N-C-500, Co-N-C-600, Co-N-C-700, Co-N-C-800, and Co-N-C-900.....	9
9. Figure S 9. XPS spectra survey scan of (a) Co_3O_4 , (b) Co-N-C-500, (c) Co-N-C-600, and (d) Co-N-C-700.	10
10. Figure S 10. XPS spectra survey scan of Co-N-C-500 after immersing.....	10
11. Figure S 11. EPR spectra of Co_3O_4	11
12. Figure S 12. (a) The TEM images and particle size distribution statistics (inset) of the Co-N-C-500. (b) The TEM images and particle size distribution statistics (inset) of the Co-N-C-700.	12
13. Figure S 13. (a) The TEM images and particle size distribution statistics (inset) of the Z-Co-N-C-900. (b) STEM and the element mapping images of Z-Co-N-C-900.	12
14. Figure S 14. LSV curves of Co_3O_4 , Co-N-C-500, Co-N-C-600, and Co-N-C-700 in 0.05 M K_2SO_4 with and without 0.05 M NO_3^-	13
15. Figure S 15. (a) NO_2^- yield rate and FE, (b) N_2H_4 absorbance, (c) NH_3 yield rate and FE, and (d) FE of NH_3 , NO_2^- , H_2 , and other by-products of Co-N-C-500 at various potentials in 0.05 M K_2SO_4 with 0.01 M NO_3^-	14
16. Figure S 16. XPS spectra survey scan of (a) Co-N-C-500-30h-after. The high-resolution XPS spectra of the Co-N-C-500 and Co-N-C-500-30h-after: (b) Co 2p, (c) C 1s, (d) N 1s, and (e) O 1s.	15
17. Figure S 17. CV curves of (a) Co_3O_4 , (b) Co-N-C-500, (c) Co-N-C-600, and (d) Co-N-C-700.	16
18. Figure S 18. Electrochemical impedance spectroscopy plot of the Co_3O_4 , (b) Co-N-C-500, (c) Co-N-C-600, and Co-N-C-700.....	17
19. Figure S 19. (a) The XRD patterns of Co-N-C-700 and immersion-1h of Co-N-C-700.....	18
20. Table S 1. The comparison of electrocatalytic NRA performance of Co-N-C-500 with other reported catalysts.....	19

Experimental Section

Materials: The ethanol was purchased from Energy chemical. The potassium sulphate (K_2SO_4 , 98%) and sodium nitrate- ^{15}N ($Na^{15}NO_3$, abundance of elements 99%) were bought from Shanghai Aladdin Ltd. The source of $Co(NO_3)_2 \cdot 6H_2O$ and potassium nitrate (KNO_3 , 98%) was Sinopharm chemical reagent Co., ltd. The sodium nitrate ($NaNO_3$, 99%) was purchased from damao chemical reagent factory. The 2-methylimidazole ($C_4H_6N_2$) was bought from Shanghai Aladdin Ltd.. The sodium sulphate (Na_2SO_4 , 99%) was obtained from 3A Materials. All chemicals were applied without further purification.

Synthesis of samples: 0.656 g 2-methylimidazole ($C_4H_6N_2$) and 0.2911 g $Co(NO_3)_2 \cdot 6H_2O$ were dissolved in 20 mL deionized water, respectively. The two solutions were then mixed under a rapid stirring. A piece of copper foam ($1 \times 1.5 \text{ cm}^2$) cleaned with acetone, ethanol and water was placed in the mixture for 12 hours at room temperature to obtain Co-MOF. The Co-MOF was calcined at 500, 600, and 700 °C for 3 hours in a nitrogen atmosphere with a ramp rate of $4 \text{ }^\circ\text{C min}^{-1}$, and the samples obtained were denoted as Co-N-C-500, Co-N-C-600, and Co-N-C-700, respectively. The Co_3O_4 was prepared under the same conditions as the preparation Co-N-C-500, except in an air atmosphere. The synthesis method of Zn-Co-MOF is consistent with that of Co-MOF. Only the raw material quantity is modified to 2.62 g 2-methylimidazole ($C_4H_6N_2$), 0.15 g $Co(NO_3)_2 \cdot 6H_2O$ and 1.34 g $Zn(NO_3)_2 \cdot 6H_2O$ and modify the amount of deionized water to 40 mL. The Zn-Co-MOF precursor was subjected to calcination at 900 °C in N_2 atmosphere, other conditions are consistent with the Co-N-C-500, and the resulting sample was designated as Z-Co-N-C-900.

Characterizations

X-ray diffraction (XRD) patterns were obtained on AXS D8ADVANCE A25 (Bruker, Germany) equipped with $Cu-K\alpha$ radiation. Scanning electron microscope (SEM) images were acquired by sigma 300 (Zeiss, Germany) cold field emission scanning electron microscope. X-ray photoelectron spectroscopy (XPS) was collected on ESCALAB Xi+. The absorbance was tested on a PERSEE TU-1901 dual-beam UV-vis spectrophotometer. The electrochemical workstation uses the CHI 660D (Shanghai CH Instruments, P. R. China). The *in-situ* attenuated total reflection Fourier-transformed infrared spectroscopy (ATR-FTIR) uses the Nicolet iS20 (Thermo Fisher

Scientific, USA) and photoelectrochemistry *in-situ* attenuated total reflection infrared reaction cell (EC-ATR-H, Beijing Scistar Technology Co. Ltd.). The transmission electron microscopy (TEM) analysis was performed on the FEI Talos F200X. The produced gas was analysed in the gas chromatograph (Tianmi GC7900, TCD, 13X columns, N₂ as carrier). The ion chromatography (IC) was tested on a Thermo Fisher Aquion. The ¹H nuclear magnetic resonance (NMR) spectrum was acquired by BRUKER AVANCEIIIHD500. The elemental composition was determined by the inductively coupled plasma optical emission spectrometer (ICP-OES, Agilent 5110).

Electrocatalytic nitrate reduction tests

The electrochemical measurements were carried on a CHI 660D in a H-typed electrolysis cell by a cation exchange membrane (Nafion 117) using a standard three-electrode setup. The saturated calomel electrode (SCE) and Pt foil were employed as the reference and counter electrodes, respectively. The K₂SO₄ and KNO₃ were electrolyte and nitrogen source, respectively. Unless otherwise stated, all the potentials reported in this work were converted to reversible hydrogen electrode (RHE) scale via calibration with the following equation: ($E_{RHE} = E_{SCE} + 0.059 \times \text{pH} + 0.242 \text{ V}$). The linear sweep voltammetry (LSV) curves were collected with a scan range from 0.654 to -0.845 V vs. RHE at a scan rate of 20 mV s⁻¹. The condition of the stability test was that the electrode remained unchanged and the electrolyte was replaced at the end of each cycle. The amount of tert-butanol added in the trap experiment was 5 mL.

Electrochemical *in-situ* ATR-FTIR test

The glassy carbon electrode supported by catalyst was used as the working electrode. 0.05 M K₂SO₄ with 200 ppm NO₃⁻-N was adopted as the electrolyte. The *in-situ* ATR-FTIR spectra were collected during LSV test from 0.65 to -0.94 V vs. RHE with a scan rate of 2 mV/s. Each reflectance spectrum was collected with a time resolution of 60 s at a spectral resolution of 4 cm⁻¹.

Determination of NO_3^- -N

First, a certain amount of electrolyte was removed from the electrolytic cell and diluted to 50 mL to the detection range. Subsequently, 1 mL 1 M HCl and 0.1 mL 0.8 wt% $\text{H}_3\text{NO}_3\text{S}$ solution were added to the above solution. The absorbance was detected by UV-Vis spectrophotometry after 15 min at a wavelength of 220 nm and 275 nm. The final absorbance of NO_3^- can be calculated as following: $A=A_{220 \text{ nm}} - 2A_{275 \text{ nm}}$. The calibration curve can be acquired through different concentrations of NaNO_3 solutions and corresponding absorbance. The fitting curve ($y = 0.2516x - 0.0012$, $R^2 = 0.9997$) exhibited great linear relation of absorbance value with NO_3^- -N concentration.

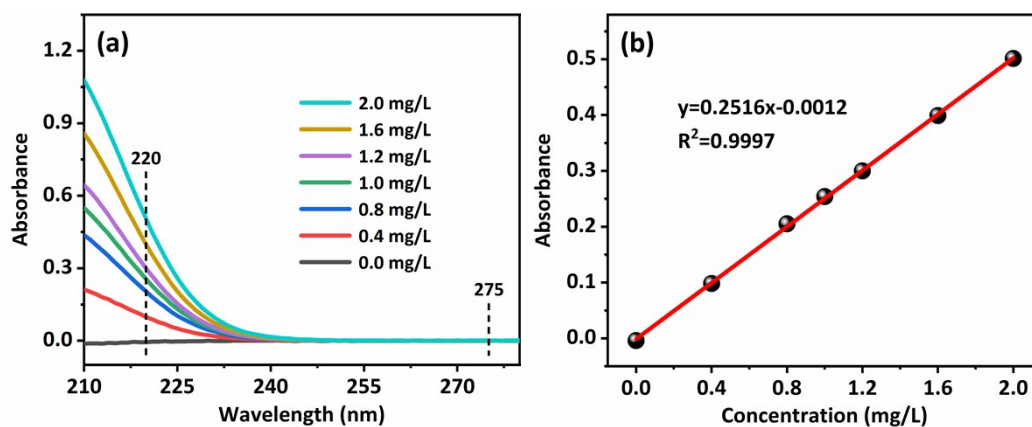


Figure S 1. (a) UV-Vis absorption curves of NO_3^- -N. (b) Calibration curve used to estimate the concentrations of NO_3^- -N.

Determination of NO_2^- -N

A mixture of p-aminobenzenesulfonamide (5 g), HCl (50 mL), and ultrapure water (450 mL) were used as a color reagent. A certain amount of electrolyte was removed from the electrolytic cell and diluted to 50 mL to the detection range. 1 mL mixed solution of p-aminobenzenesulfonamide and HCl and 1 mL N-(1-Naphthyl) ethylenediamine dihydrochloride (1 g/L) were added into the above solution and mixed uniformly. After standing at room temperature for 20 min, the absorbance was recorded at a wavelength of 540 nm. The concentration-absorbance curve was calibrated using the standard NaNO_2 with different NO_2^- -N concentrations. The fitting curve ($y = 3.12x + 0.0597$, $R^2 = 0.9999$) exhibited great linear relation of absorbance value with NO_2^- -N concentration.

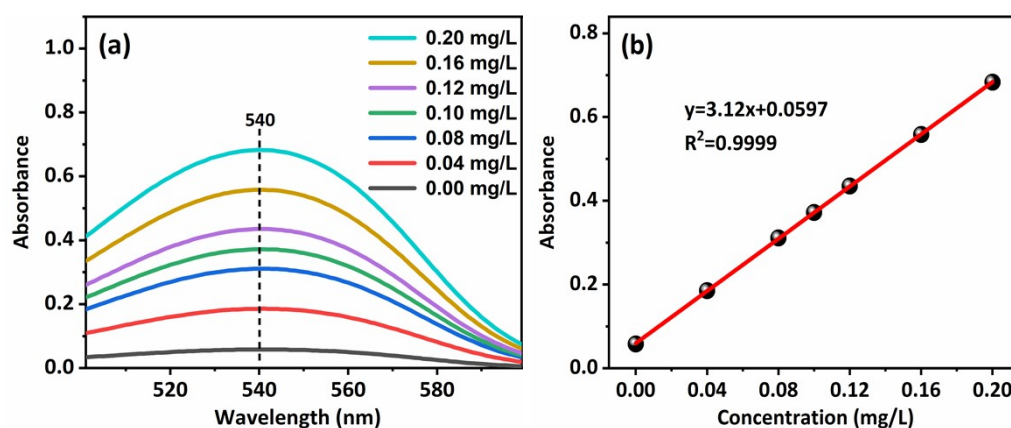


Figure S 2. (a) UV-Vis absorption curves of NO_2^- -N. (b) Calibration curve used to estimate the concentrations of NO_2^- -N.

Determination of N₂H₄-N

The N₂H₄ concentration was analyzed by Watt-Chrisp method. A mixture of C₉H₁₁NO (4.0 g), HCl (concentrated, 20.0 mL) and 95% ethanol (200 mL) was used as a color reagent. A certain amount of electrolyte was removed from the electrolytic cell and diluted to 25 mL to the detection range. 5 mL of color reagent were added into the above solution and mixed uniformly. After standing at room temperature for 20 min, the absorbance was recorded at a wavelength of 458 nm. The concentration absorbance curves were calibrated using a standard N₂H₄·H₂O solution with a series of concentrations. The fitting curve ($y = 1.6046x - 0.0682$, $R^2 = 0.9993$) exhibited great linear relation of absorbance value with N₂H₄ concentration.

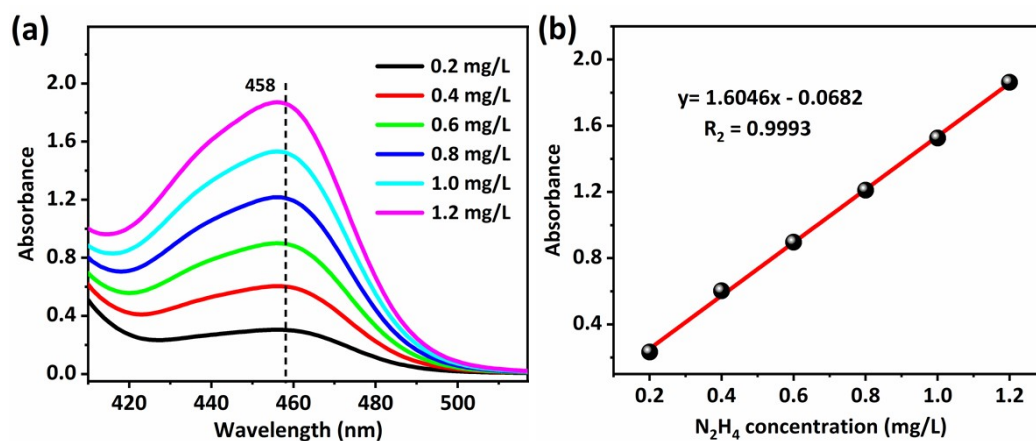


Figure S 3. (a) UV-Vis curves of various concentrations of N₂H₄ stained with C₉H₁₁NO indicator. (b) A calibration curve used to estimate the concentrations of N₂H₄.

Determination of $\text{NH}_3\text{-N}$ (Nessler's reagent)

The Nessler's reagent was employed as the color reagent for the determination of $\text{NH}_3\text{-N}$. Firstly, a certain amount of electrolyte was removed from the electrolytic cell and diluted to 50 mL to the detection range. Then, 1 mL of potassium sodium tartrate solution and 1 mL Nessler's reagent were subsequently added into the above solution and mixed uniformly. After standing at room temperature for 20 min, the absorbance was recorded at a wavelength of 420 nm. The concentration-absorbance curve was calibrated using the standard NH_4Cl with different $\text{NH}_4^+\text{-N}$ concentrations. The fitting curve ($y = 0.1753x + 0.0122$, $R^2 = 0.999$) exhibited great linear relation of absorbance value with $\text{NH}_4^+\text{-N}$ concentration.

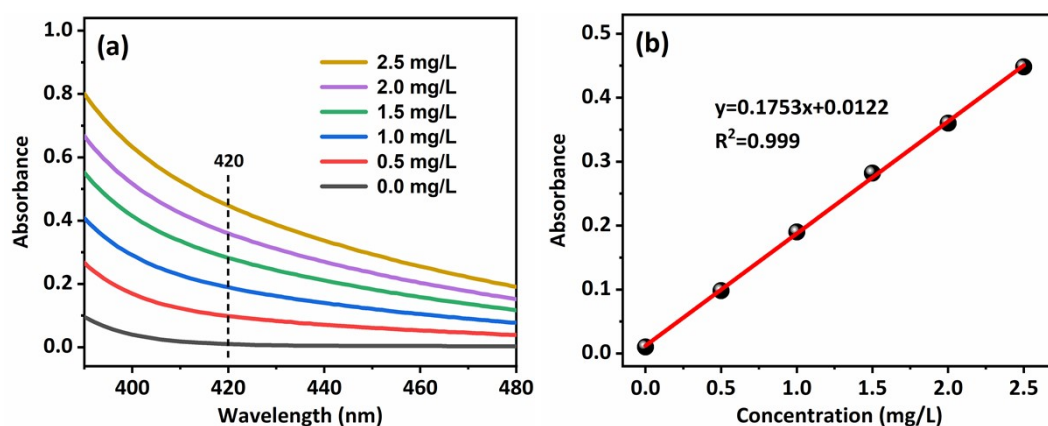


Figure S 4. (a) UV-Vis absorption curves of Nessler's reagent assays kept with different concentrations of $\text{NH}_4^+\text{-N}$. (b) Calibration curve used to estimate the concentrations of $\text{NH}_4^+\text{-N}$.

Determination of NH₃-N (Ion chromatography)

The standard curve was prepared by external standard method using NH₄Cl as standard solution.

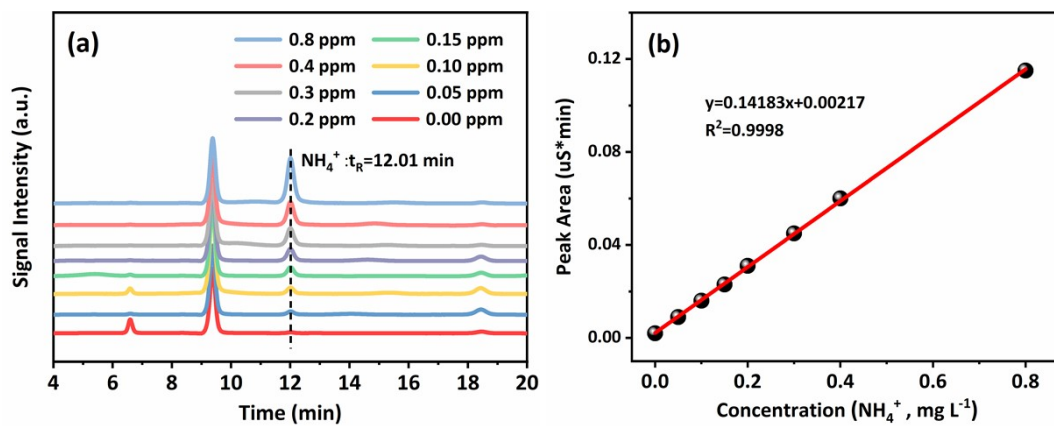


Figure S 5. The NH₄⁺ detection of (a) standard spectra and (b) fitting curve by ion chromatography.

Determination of H₂

The standard curve was prepared by external standard method using high purity H₂ as standard gas ($y = 496542x$, $R^2 = 0.999$).

Calculations of FE and NH₃ yield

$$FE = (8 \times F \times C_{NH_3} \times V) \div (M_{NH_3} \times Q) \times 100\%$$

$$NH_3 \text{ yield} = (C_{NH_3} \times V) \div (M_{NH_3} \times t \times S)$$

Where F is the Faradic constant (96485 C mol^{-1}), C_{NH_3} is the measured NH₃ concentration, V is the volume of electrolyte in the anode compartment (80 mL), M_{NH_3} is the molar mass of NH₃, Q is the total quantity of applied electricity, t is the electrolysis time (1 h), S is the loaded area of catalyst (1 cm^2).

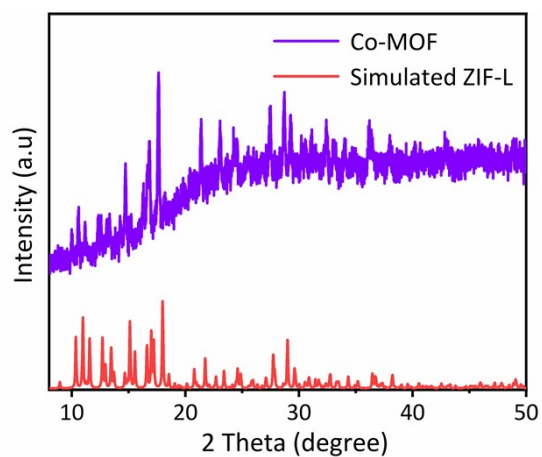


Figure S 6. The XRD patterns of the Co-MOF precursor. Simulated data of ZIF-L (Deposition Number: 1509273) from the Inorganic Crystal Structure Database (ICSD).

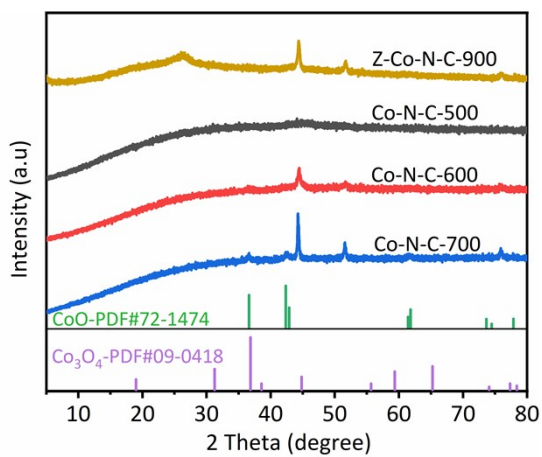


Figure S 7. The XRD patterns of the Co-N-C-500, Co-N-C-600, Co-N-C-700, and Z-Co-N-C-900.

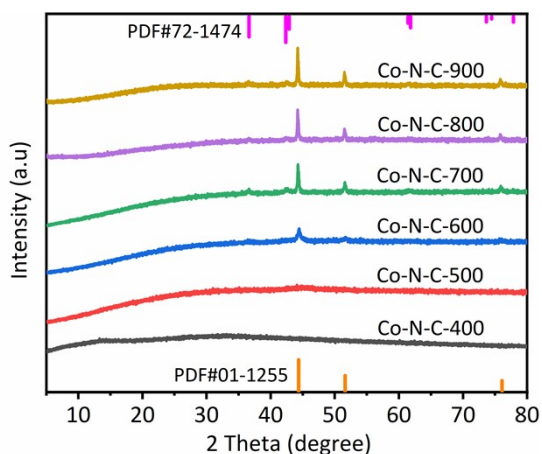


Figure S 8. The XRD patterns of the Co-N-C-400, Co-N-C-500, Co-N-C-600, Co-N-C-700, Co-N-C-800, and Co-N-C-900.

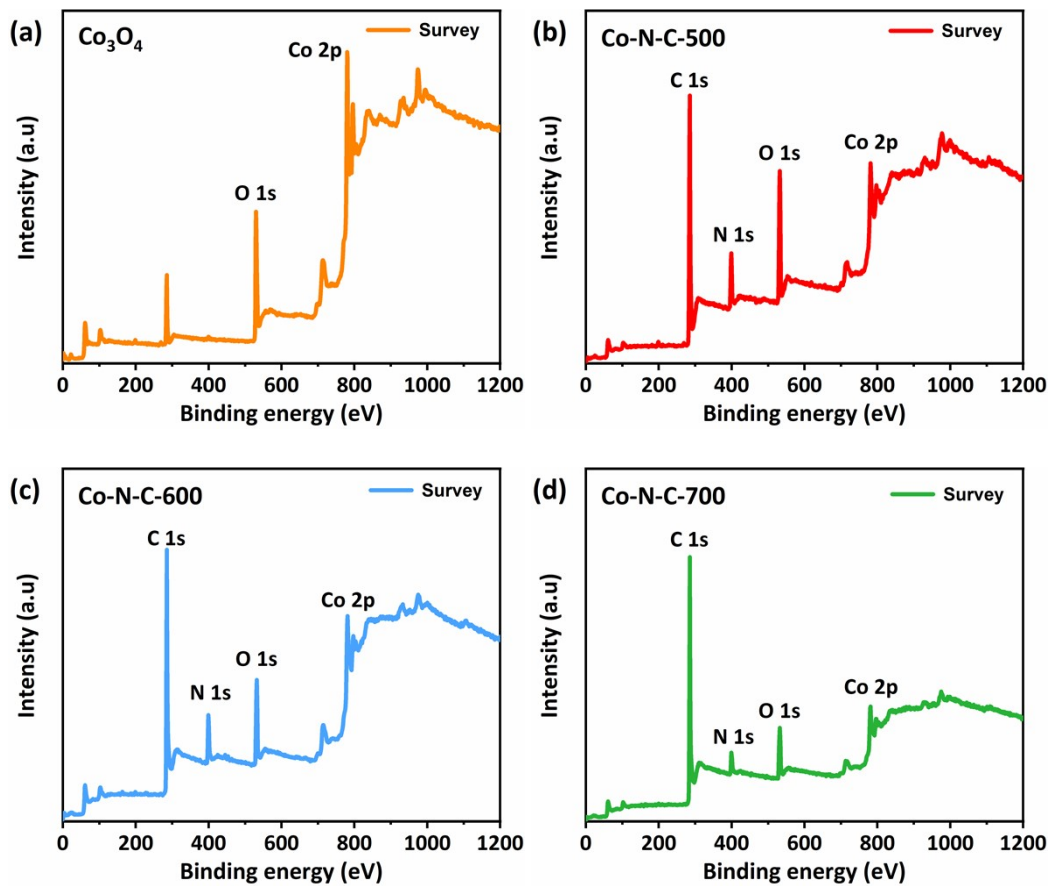


Figure S 9. XPS spectra survey scan of (a) Co_3O_4 , (b) Co-N-C-500, (c) Co-N-C-600, and (d) Co-N-C-700.

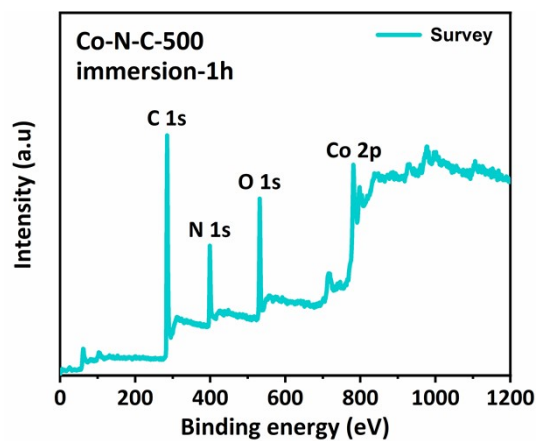


Figure S 10. XPS spectra survey scan of Co-N-C-500 after immersing

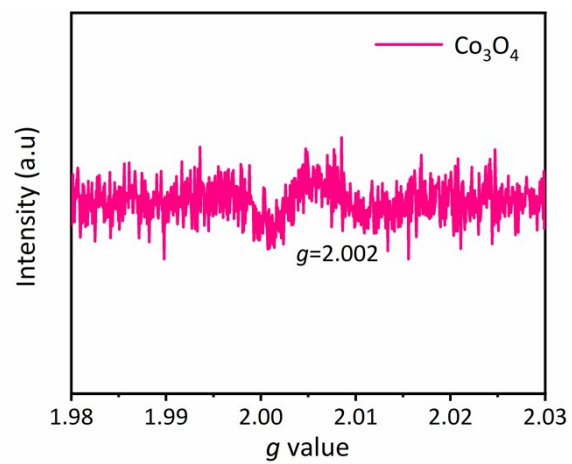


Figure S 11. EPR spectra of Co_3O_4

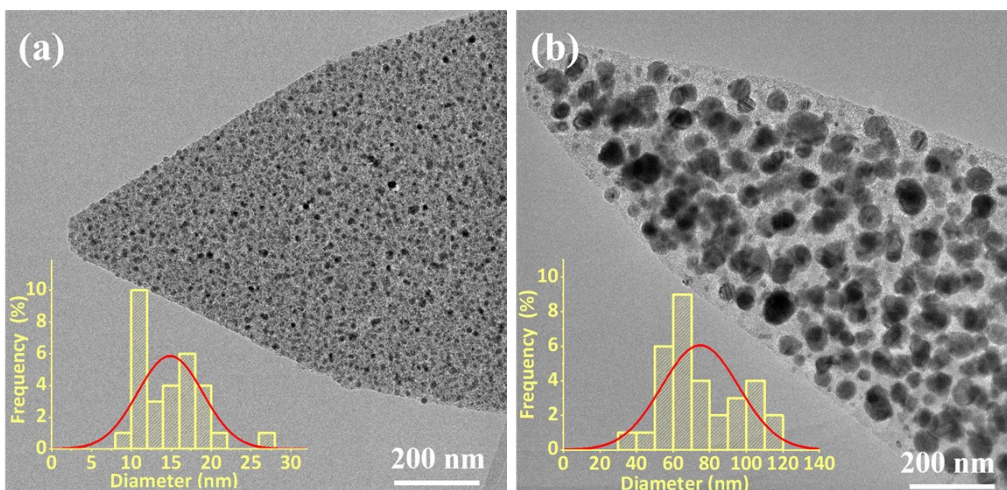


Figure S 12. (a) The TEM images and particle size distribution statistics (inset) of the Co-N-C-500. (b) The TEM images and particle size distribution statistics (inset) of the Co-N-C-700.

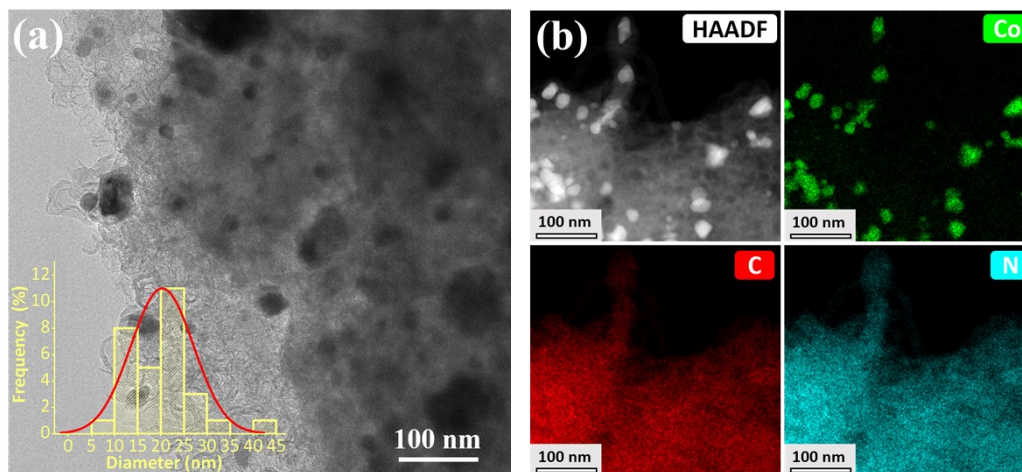


Figure S 13. (a) The TEM images and particle size distribution statistics (inset) of the Z-Co-N-C-900. (b) STEM and the element mapping images of Z-Co-N-C-900.

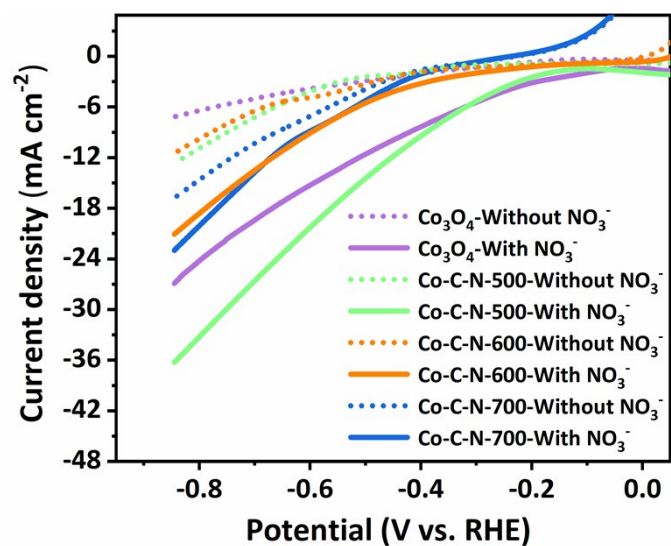


Figure S 14. LSV curves of Co₃O₄, Co-N-C-500, Co-N-C-600, and Co-N-C-700 with a scan rate of 20 mV/s in 0.05 M K₂SO₄ with and without 0.05 M NO₃⁻.

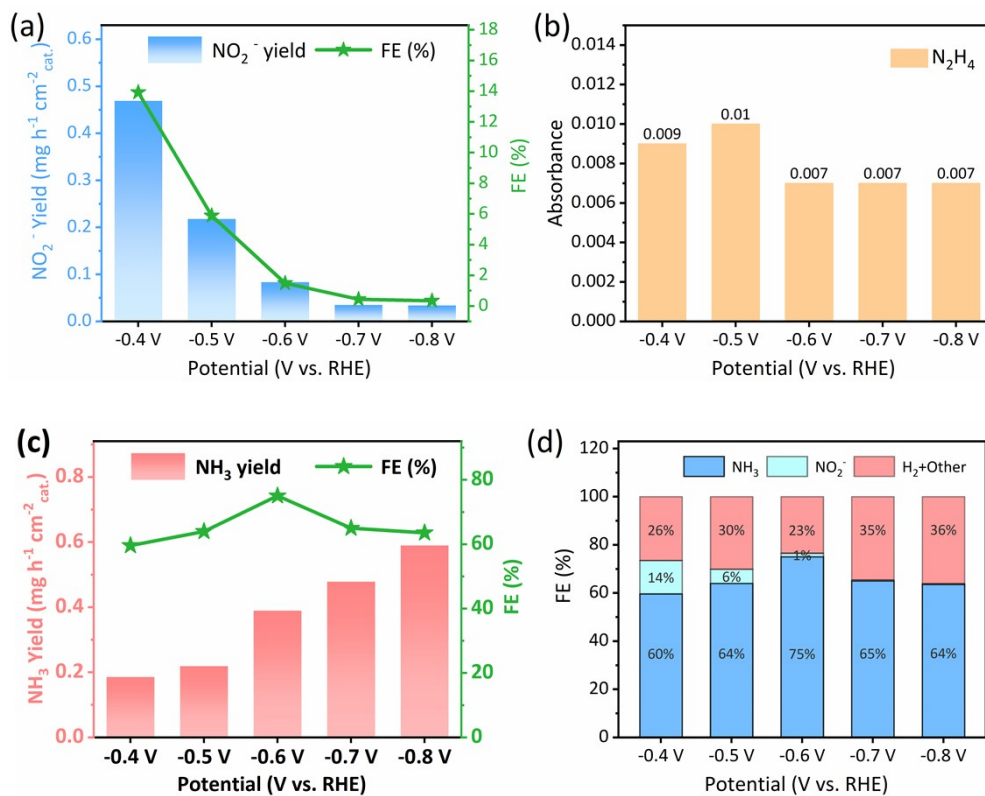


Figure S 15. (a) NO₂⁻ yield rate and FE, (b) N₂H₄ absorbance, (c) NH₃ yield rate and FE, and (d) FE of NH₃, NO₂⁻, H₂, and other by-products of Co-N-C-500 at various potentials in 0.05 M K₂SO₄ with 0.01 M NO₃⁻.

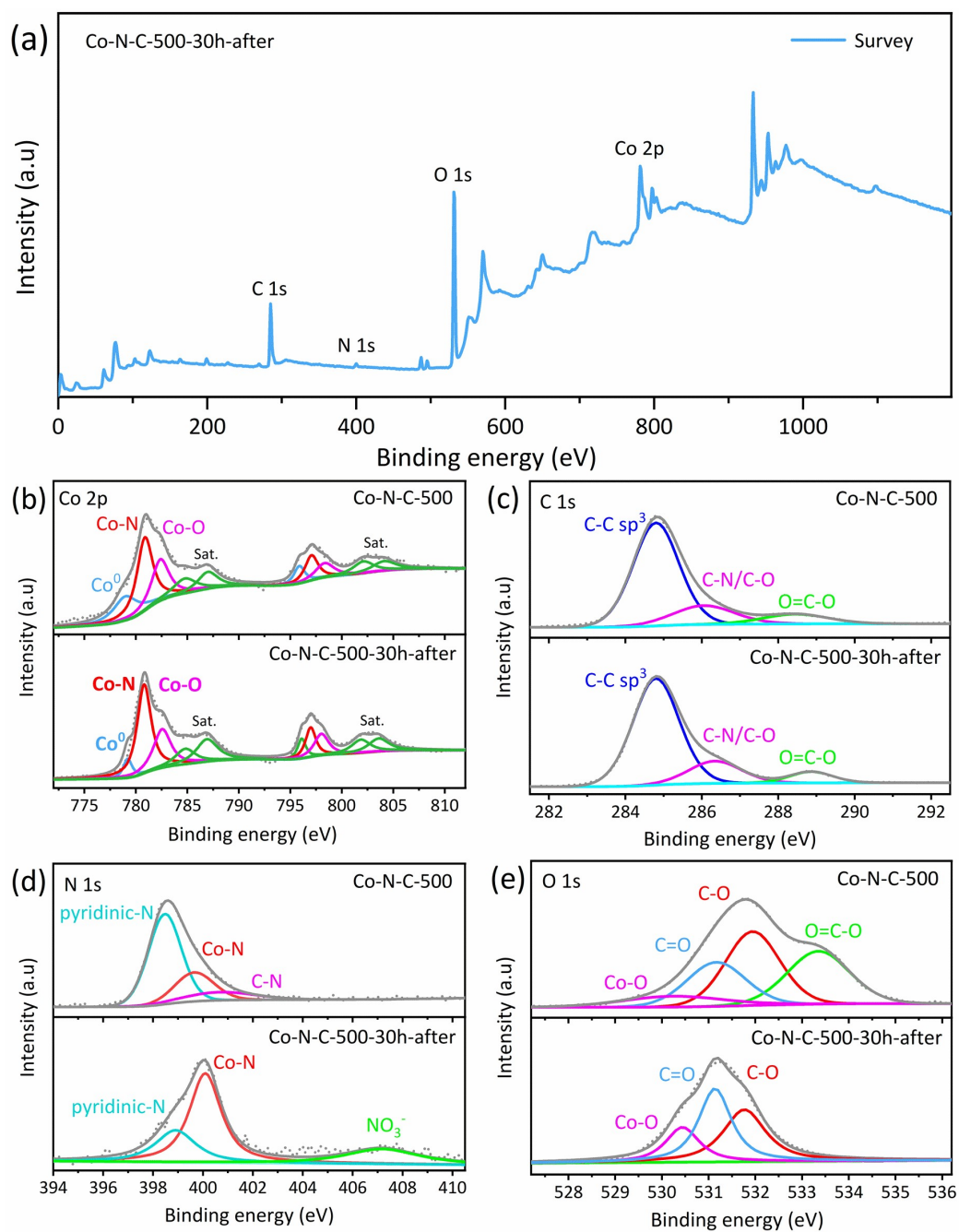


Figure S 16. XPS spectra survey scan of (a) Co-N-C-500-30h-after. The high-resolution XPS spectra of the Co-N-C-500 and Co-N-C-500-30h-after: (b) Co 2p, (c) C 1s, (d) N 1s, and (e) O 1s.

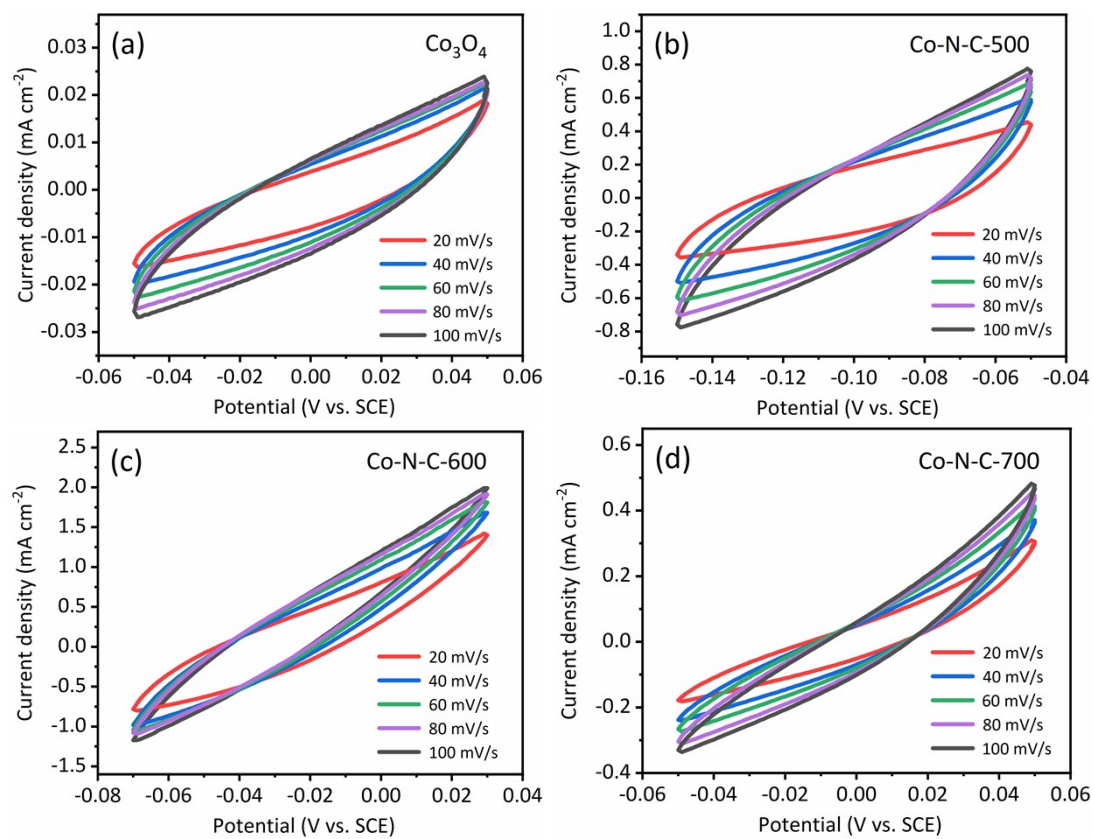


Figure S 17. CV curves of (a) Co₃O₄, (b) Co-N-C-500, (c) Co-N-C-600, and (d) Co-N-C-700.

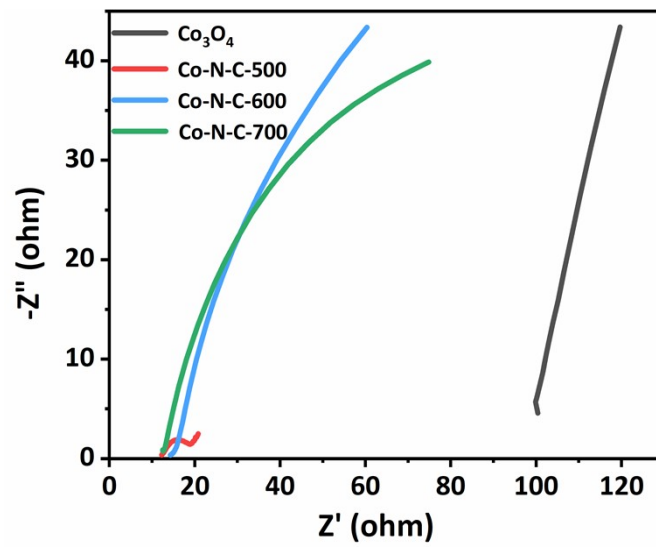


Figure S 18. Electrochemical impedance spectroscopy plot of the Co_3O_4 , (b) Co-N-C-500, (c) Co-N-C-600, and Co-N-C-700

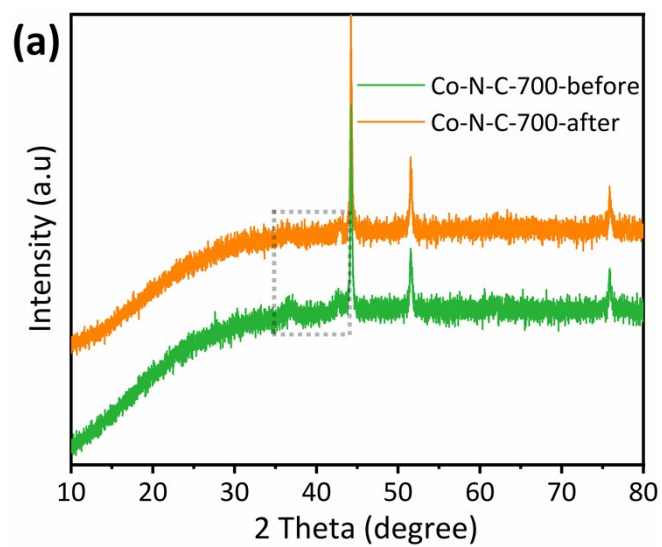


Figure S 19. (a) The XRD patterns of Co-N-C-700 and immersion-1h of Co-N-C-700.

The amount of catalyst used in the **Figure 6b** was 20 mg. The amount of catalyst used in the **Figure S19** was 50 mg.

Table S 1. The comparison of electrocatalytic NRA performance of Co-N-C-500 with other reported catalysts.

Catalyst	Applied potential	Electrolyte	NH ₃ yield	FE (%)	Ref.
Co-N-C-500	-0.8 V (vs. RHE)	0.05 M Na₂SO₄/0.1 M NO₃⁻-N	2.8 mg h⁻¹ cm⁻²	86.8	This work
Co-N-C	-0.6 V (vs. RHE)	0.05 M PBS/0.16 M KNO ₃	14 μmol h ⁻¹ cm ⁻²	50	1
Co-CN	-0.69 V (vs. RHE)	0.02 M Na ₂ SO ₄ /100 mg/L NO ₃ ⁻ -N	0.43 mg h ⁻¹ cm ⁻²	87	2
PP-Co	-0.6 V (vs. RHE)	0.1 M NaOH/0.1 M NO ₃ ⁻	1.1 mmol h ⁻¹ mg _{cat.} ⁻¹	90.1	3
Co@CC	-0.8 V (vs. RHE)	0.1 M NaOH/0.1 M NO ₃ ⁻	0.6 mmol h ⁻¹ mg _{cat.} ⁻¹	93.4	4
Ni@JBC-800	-0.5 V (vs. RHE)	0.1 M NaOH/0.1 M NO ₂ ⁻	4.12 mg h ⁻¹ mg _{cat.} ⁻¹	83.4	5
Ni-N-C	-0.6 V (vs. RHE)	0.05 M PBS/0.16 M KNO ₃	0.74 mg h ⁻¹ mg _{cat.} ⁻¹	25	1
Ni-NC	-0.70 V (vs. RHE)	0.5 M Na ₂ SO ₄ /100 mg/L NaNO ₃	-	15.2	6
Cu/JDC/CP	-0.6 V (vs. RHE)	0.1 M NaOH/0.1 M NO ₂ ⁻	0.52 mmol h ⁻¹ mg _{cat.} ⁻¹	93.2	7
Cu/Ni-NC	-0.70 V (vs. RHE)	0.5 M Na ₂ SO ₄ /100 mg/L NaNO ₃	5.48 mg h ⁻¹ cm ⁻²	97	6
Cu(I)-N ₃ C ₁	-0.64 V (vs. RHE)	0.05 M Na ₂ SO ₄ /500 mg/L NO ₃ ⁻ -N	80 μmol h ⁻¹ mg _{cat.} ⁻¹	94	8
Cu-N-C SAC	-1.0 V (vs. RHE)	0.1 M KOH/0.1 M KNO ₃	4.5 mg h ⁻¹ cm ⁻²	84.7	9
Cu-NC	-0.70 V (vs. RHE)	0.5 M Na ₂ SO ₄ /100 mg/L NaNO ₃	-	33.2	6
Cu SAGs	-0.8 V (vs. RHE)	0.1 M PBS/20 mM NO ₃ ⁻	0.44 mg h ⁻¹ cm ⁻²	78	10
Cu-GS-800	-0.8 V (vs. RHE)	0.1 M K ₂ SO ₄ /0.1 M KNO ₃	2.2 mg h ⁻¹ mg _{cat.} ⁻¹	59	11
Fe SAC	-0.66 V (vs. RHE)	0.1 M K ₂ SO ₄ /0.5 M KNO ₃	5.24 mg h ⁻¹ mg _{cat.} ⁻¹	75	12

Fe-N-C	-0.45 V (vs. RHE)	0.05 M PBS/0.16 M NO ₃ ⁻	10 μmol h ⁻¹ cm ⁻²	82	13
Mo-N-C	-0.45 V (vs. RHE)	0.05 M PBS/0.16 M NO ₃ ⁻	5 μmol h ⁻¹ cm ⁻²	62	13
FeMo-N-C	-0.45 V (vs. RHE)	0.05 M PBS/0.16 M NO ₃ ⁻	17 μmol h ⁻¹ cm ⁻²	93	13

References

1. E. Murphy, Y. Liu, I. Matanovic, M. Rüscher, Y. Huang, A. Ly, S. Guo, W. Zang, X. Yan, A. Martini, J. Timoshenko, B. R. Cuenya, I. V. Zenyuk, X. Pan, E. D. Spoecke and P. Atanassov, *Nature Communications*, 2023, **14**.
2. J. Li, M. Li, N. An, S. Zhang, Q. Song, Y. Yang, J. Li and X. Liu, *Proceedings of the National Academy of Sciences*, 2022, **119**.
3. Q. Chen, J. Liang, Q. Liu, K. Dong, L. Yue, P. Wei, Y. Luo, Q. Liu, N. Li, B. Tang, A. A. Alshehri, M. S. Hamdy, Z. Jiang and X. Sun, *Chem Commun (Camb)*, 2022, **58**, 4259-4262.
4. T. Xie, X. Li, J. Li, J. Chen, S. Sun, Y. Luo, Q. Liu, D. Zhao, C. Xu, L. Xie and X. Sun, *Inorg Chem*, 2022, **61**, 14195-14200.
5. X. Li, Z. Li, L. Zhang, D. Zhao, J. Li, S. Sun, L. Xie, Q. Liu, A. A. Alshehri, Y. Luo, Y. Liao, Q. Kong and X. Sun, *Nanoscale*, 2022, **14**, 13073-13077.
6. Y. Wang, H. Yin, F. Dong, X. Zhao, Y. Qu, L. Wang, Y. Peng, D. Wang, W. Fang and J. Li, *Small*, 2023, **19**.
7. L. Ouyang, L. Yue, Q. Liu, Q. Liu, Z. Li, S. Sun, Y. Luo, A. Ali Alshehri, M. S. Hamdy, Q. Kong and X. Sun, *J Colloid Interface Sci*, 2022, **624**, 394-399.
8. Y. Xue, Q. Yu, Q. Ma, Y. Chen, C. Zhang, W. Teng, J. Fan and W. X. Zhang, *Environ Sci Technol*, 2022, **56**, 14797-14807.
9. J. Yang, H. Qi, A. Li, X. Liu, X. Yang, S. Zhang, Q. Zhao, Q. Jiang, Y. Su, L. Zhang, J.-F. Li, Z.-Q. Tian, W. Liu, A. Wang and T. Zhang, *Journal of the American Chemical Society*, 2022, **144**, 12062-12071.
10. P. Li, R. Li, Y. Liu, M. Xie, Z. Jin and G. Yu, *Journal of the American Chemical Society*, 2023, **145**, 6471-6479.
11. J. Leverett, T. Tran-Phu, J. A. Yuwono, P. Kumar, C. Kim, Q. Zhai, C. Han, J. Qu, J. Cairney, A. N. Simonov, R. K. Hocking, L. Dai, R. Daiyan and R. Amal, *Advanced Energy Materials*, 2022, **12**.
12. Z. Y. Wu, M. Karamad, X. Yong, Q. Huang, D. A. Cullen, P. Zhu, C. Xia, Q. Xiao, M. Shakouri, F. Y. Chen, J. Y. T. Kim, Y. Xia, K. Heck, Y. Hu, M. S. Wong, Q. Li, I. Gates, S. Siahrostami and H. Wang, *Nat Commun*, 2021, **12**, 2870.
13. E. Murphy, Y. Liu, I. Matanovic, S. Guo, P. Tieu, Y. Huang, A. Ly, S. Das, I. Zenyuk, X. Pan, E. Spoecke and P. Atanassov, *ACS Catalysis*, 2022, **12**, 6651-6662.